Classical charge-transfer and ionization channels for ion collisions with circular Rydberg atoms

Dean M. Homan, Michael J. Cavagnero, and David A. Harmin
Department of Physics and Astronomy, University of Kentucky, Lexington, Kentucky 40506-0055
(Received 25 July 1994)

Explorations of the classical phase space for ion collisions with circular Rydberg atoms are presented. Intermediate-energy capture and ionization processes are studied through the numerical integration of Newton's equations of motion and through the graphical depiction of the outcomes of large numbers of trajectories. Maps which correlate initial conditions with final outcomes are used to identify zones of parameter space leading to Thomas capture, direct capture, binary-encounter ionization, saddle-point ionization, and ionization by S superpromotion (E. A. Solov'ev, Zh. Eksp. Teor. Fiz. **81**, 1681 (1981) [Sov. Phys. JETP **54**, 893 (1981)]). Charge-transfer channels in which the electron passes once or three times through the midplane between the nuclei are shown to occur in separate zones of parameter space over the entire range of projectile speeds above the mean velocity of the target electron.

PACS number(s): 34.10.+x, 34.60.+z, 34.70.+e, 34.80.Dp

I. INTRODUCTION

Collisions of singly charged projectiles with alkali-metal atoms in prepared Rydberg states probe weakly bound electronic states of a transient molecular-ion complex. Charge-transfer measurements from singly charged alkali-metal ions to laser-excited alkali-metal atom targets were initiated about 1980 [1], but remain largely beyond the scope of ion-atom collision theory. Difficulties in the theory stem from the accessibility of many manifolds of nearly degenerate states with disparate geometric and dynamic characteristics. The utility of an adiabatic (or fixed-nuclei) representation of such collisions, the mainstay of ion-atom collision theory, is in doubt due to the small energy splittings and high degree of degeneracy of target states.

Recent progress in this field stems from the experimental production of target states of a Rydberg atom that mimic circular [2,3] and elliptic [4] classical orbits. These states are produced by laser excitation in the presence of perpendicular electric and magnetic fields. The fields can be manipulated to orient the states in arbitrary directions and to vary their (mean) eccentricity. With the advent of this crossed-field method of target preparation, it is now possible to study the interaction of a charged projectile with an oriented Rydberg atom in a stationary state that is localized in both position and momentum space about a single Kepler orbit [5–7]. These experiments invite comparison of measured cross sections with purely classical descriptions of the collision process [8].

We recently presented a model study of charge-transfer cross sections for ion collisions with circular and elliptic state targets [9]. An elementary atomic model consisting of an electron in a single Kepler orbit resulted in cross sections remarkably similar to the experimental values reported in Refs. [5] and [7]. We also resolved the capture cross section into two contributions from direct capture processes and Thomas-like captures, which we labeled as one-swap and three-swap, respectively. The number of swaps is defined as the number of times the electron passes through the midplane between the two positive charge centers.

In this paper, we present a much more detailed view of the three-body mechanics of charged particle collisions with target atoms in circular orbits. We focus on coplanar trajectories that result from an initially circular orbit of the target electron and we vary the initial phase of the electron in its cycle, the impact parameter, and the collision velocity. The collision channels for ionization, excitation, and charge transfer form well defined zones in this parameter space that evolve smoothly from simple forms at high projectile velocity to more complex structures at low velocity. A number of these collision channels have quantum analogs that have been identified in previous investigations of ion-atom collisions. In this paper we will isolate regions of parameter space that correspond to these processes and identify the dominant collision channels contributing to charge transfer and ionization in ion collisions with circular-state atoms.

Classical estimates of ion-atom collision cross sections have been common since the work of Abrines and Percival [10]. The classical trajectory Monte Carlo (CTMC) method models atomic targets by using an ensemble of classical orbits that represents the spatial and/or momentum probability distribution of the target wave function [11,12]. Monte Carlo sampling of the initial conditions of the target electron and ion beam, followed by direct numerical integration of Newton's equations of motion, yields classical values for collision cross sections. This method has been successful in the intermediate velocity regime [13], where the ion and target electron speeds are comparable and where realistic quantum-mechanical calculations are difficult to perform.

This paper departs from the CTMC approach by focusing on the identification of specific pathways for each reaction process. Identifying such pathways requires a much more detailed view of small portions of the phase space than is used in the random sampling appropriate to a Monte Carlo study. We follow Thomas [14] and Wannier [15] in using Newton's laws to understand the limita-

tions that energy and momentum conservation impose on complex reaction dynamics. This is achieved by the construction and analysis of parameter space maps that correlate initial conditions with final outcomes. (Parameter space maps have been used elsewhere [16], particularly in investigations of few-body scattering for application to astronomical systems [17–19].) While these maps become very complicated at low ion velocities, we find that at velocities near and above the initial speed of the target electron the zones of parameter space associated with different reaction processes are *few in number* and *easily distinguishable.* This observation implies that large statistical calculations can, with little modification of existing codes, be adapted to distinguish among alternative contributions to capture and ionization cross sections.

In Sec. II we outline the numerical method used to integrate the electron's equations of motion. In Sec. III we define orbital parameters and the scheme used to map the parameter space onto the various collisional events. Collision channels identified by the parameter space maps are described in Sec. IV. Our conclusions are summarized in Sec. V.

II. NUMERICAL METHOD

Our approach has been to solve Newton's equations of motion for an electron in an initially circular orbit about an infinitely massive, singly charged nucleus. The projectile ion was also considered infinitely massive and so moved along a straight line at constant speed V_p. As will be demonstrated in Sec. IV D, neglecting the deflection of the projectile ion at intermediate velocities is an excellent approximation for the $Na^+ + Li^*$ collision system studied in the experiments of Refs. [5] and [7]. As a result of these assumptions, Newton's equations were reduced to a set of six coupled first-order differential equations for the Cartesian coordinates and momenta of the electron relative to the target nucleus. These equations were solved numerically subject to initial conditions that are correlated to specific outcomes, as described in the following section.

To solve the coupled equations, we used an adaptive-stepsize Runge-Kutta algorithm [20]. Initial conditions were specified at time

$$t=-t_0=-40\frac{r_0}{V_p}=-\frac{40}{\bar{v}}\frac{r_0}{v_0}\ , \tag{1}$$

where r_0 and v_0 are the initial radius and speed of the electron's circular orbit, and $\bar{v}$ is the *reduced velocity,* or the speed of the projectile ion in units of v_0. The equations of motion were then integrated up to a final time $t_f=|t_0|$. With the unit of time defined as the ratio r_0/v_0, where v_0 is the initial velocity of the target electron, we found that maximum and minimum bounds on the stepsize of $\Delta t_{\max}=0.1$ and $\Delta t_{\min}=10^{-6}$ were sufficient to produce accurate trajectories for all but a small percentage of initial conditions. Even at this level, however, a few trajectories passed sufficiently close to one of the nuclei to result in an error in the algorithm. The value of $\Delta t_{\min}$ given above was selected to ensure that the number of such errant trajectories was a small fraction of the total number ($\sim 10^{-3}$).

III. PARAMETER SPACE MAPS

A. Initial conditions

The objective of this study is to correlate initial conditions of the target and projectile with various categories of scattering outcomes. The projectile ion displacement from the target nucleus is described by the trajectory

$$\mathbf{R}(t)=V_p t\hat{\mathbf{i}}+b\hat{\mathbf{j}}\ , \tag{2}$$

where b is the impact parameter and $-t_0\le t\le t_f$. The initial conditions for a circular orbit are given by its initial radius r_0, a reference phase ϕ of the electron in its orbit (specified below), and the orientation of its angular momentum $\hat{\mathbf{l}}$ with respect to the $(\hat{\mathbf{i}},\hat{\mathbf{j}},\hat{\mathbf{k}})$ Cartesian unit vectors defined by Eq. (2). (Since b is defined as the y component of $\mathbf{R}$, it may be either positive or negative). In this paper, we only present results for coplanar collisions for which $\hat{\mathbf{l}}$ is parallel to $\hat{\mathbf{k}}$ (see the discussion in Sec. V).

To aid in correlating initial conditions with final outcomes, we follow Ref. [18] and plot parameter space maps for each value of the reduced velocity $\bar{v}$. For each $\bar{v}$, the impact parameter b and phase ϕ of the electron in its circular orbit are varied systematically and a collision outcome (described below) is determined. The outcome for each trajectory is imaged as a color pixel on a two-dimensional map, as shown in Fig. 1. Each of these maps displays the outcomes of 250 000 separately calculated trajectories, where each pixel represents a unique trajectory.

The color table shown in Fig. 1(a) assigns *blue* pixels to initial conditions that result in ionization, *red* pixels to initial conditions that result in charge transfer (capture), and *green* pixels to initial conditions that result in inelastic collisions. Further divisions among capture and inelastic collision events are represented by shades, corresponding to the number of times the electron crosses the midplane between the nuclei (number of "swaps") for each trajectory. The number of swaps for any *inelastic scattering* process is an *even* integer, with the lightest shade of green corresponding to trajectories with the largest number of swaps. For *capture* the number of swaps is *odd,* with the darkest shade of red representing one-swap trajectories, and lighter shades representing a large number (3 and 5) of swaps.

The blue ionization region is also subdivided into three regions defined by the coordinate center—target, projectile, or saddle point—with respect to which the electron is moving most slowly following the collision. The darkest shade of blue represents those trajectories for which the final electron speed is slowest with respect to the saddle point; we refer to these events as "saddle-point ionizations." The next lightest shade corresponds to those trajectories for which final electron speeds are slowest with respect to the target; these are referred to as "direct ionizations." The lightest shade represents those trajectories for which the final electron speed is slowest with respect

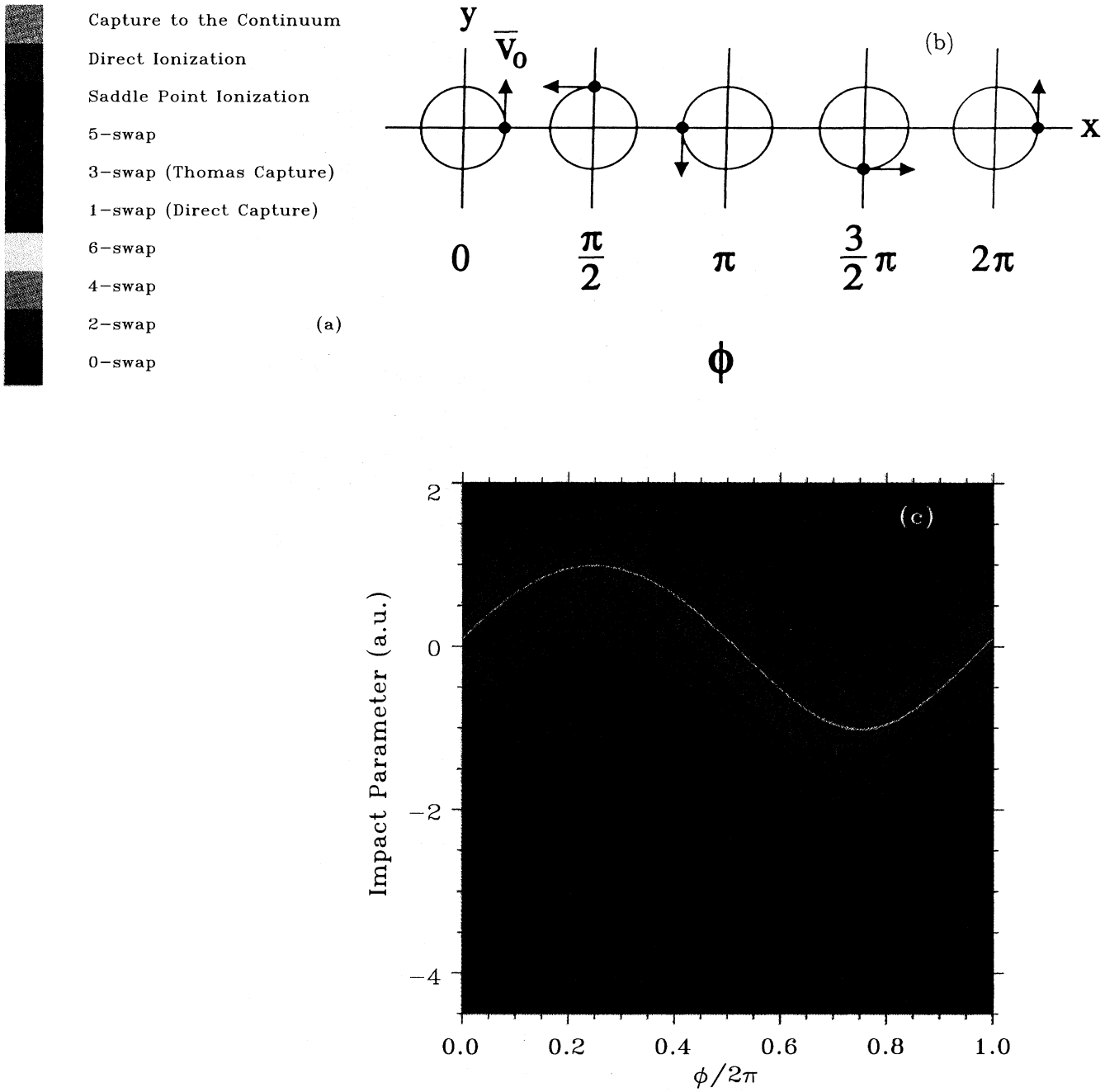

FIG. 1. Parameter space maps for coplanar collisions. These plots correlate the impact parameter and the initial phase angle ϕ of the electron's circular orbit with specific outcomes as specified in the color chart (a). The phase angle ϕ of the electron is standardized [Eq. (4)] so that, in the absence of projectile target interaction, the electron position at $t=0$ would be as shown in (b). Collision outcomes represented by a color pixel for each of 250 000 trajectories are shown for reduced ion velocities of (c) $\bar{v}=10.0$, (d) $\bar{v}=4.0$, (e) $\bar{v}=2.0$, (f) $\bar{v}=1.0$, and (g) $\bar{v}=0.5$.

to the projectile ion; this is generally referred to as "capture to the continuum."

As noted above, the variable ϕ plotted in Fig. 1 is related to the initial phase of the electron in its circular orbit. The interpretation of the parameter space maps is aided considerably by standardizing this angle in accord with the following convention. The phase angle at time $t=-t_0$ is

$$\phi_0=\cos^{-1}[\hat{\mathbf{i}}\cdot\hat{\mathbf{r}}(-t_0)]\ , \tag{3}$$

where $\hat{\mathbf{i}}$ is the beam axis and $\mathbf{r}(t)$ is the electron displacement with respect to the target nucleus. The angle plot-

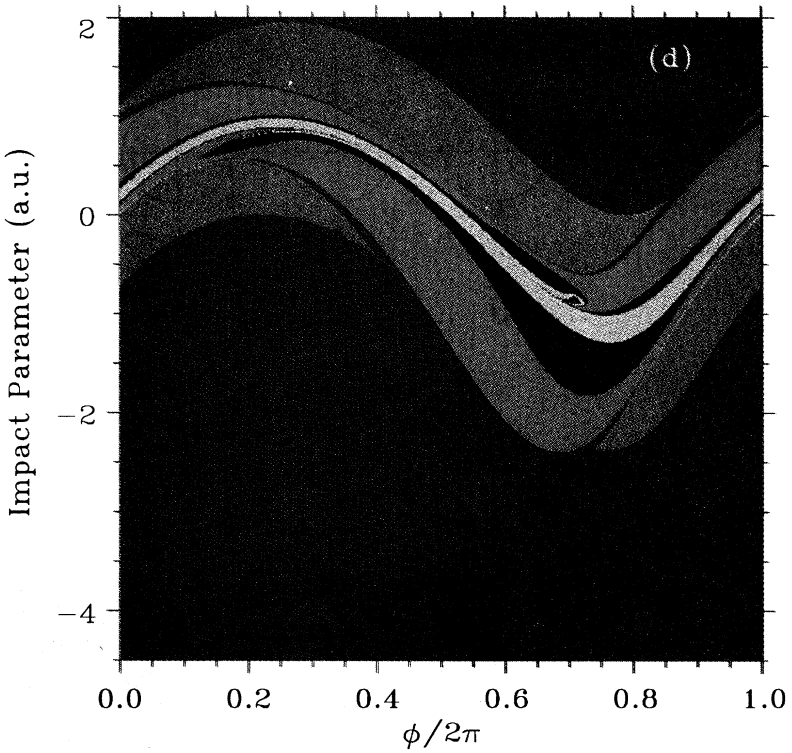

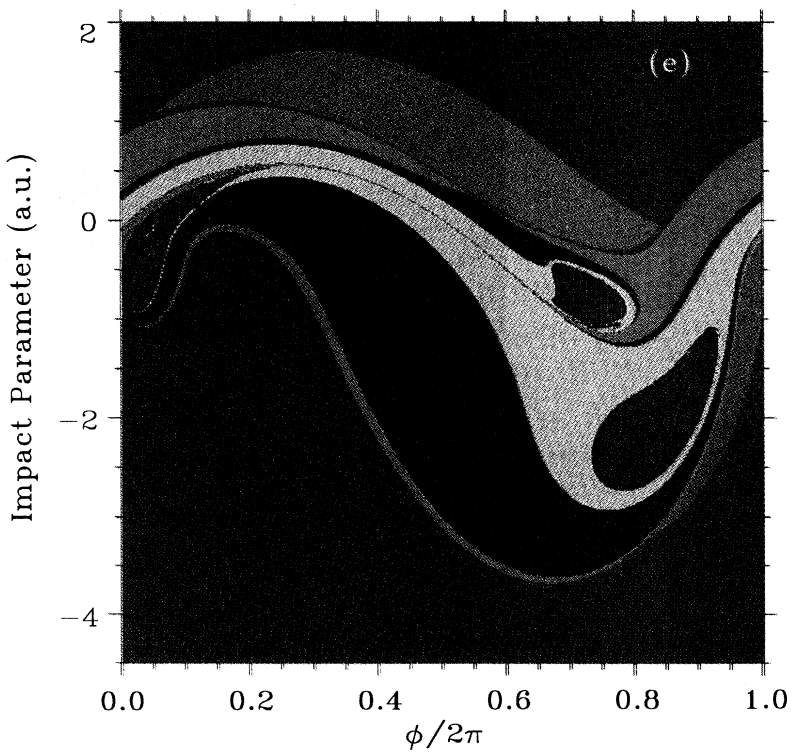

FIG. 1. (*Continued*).

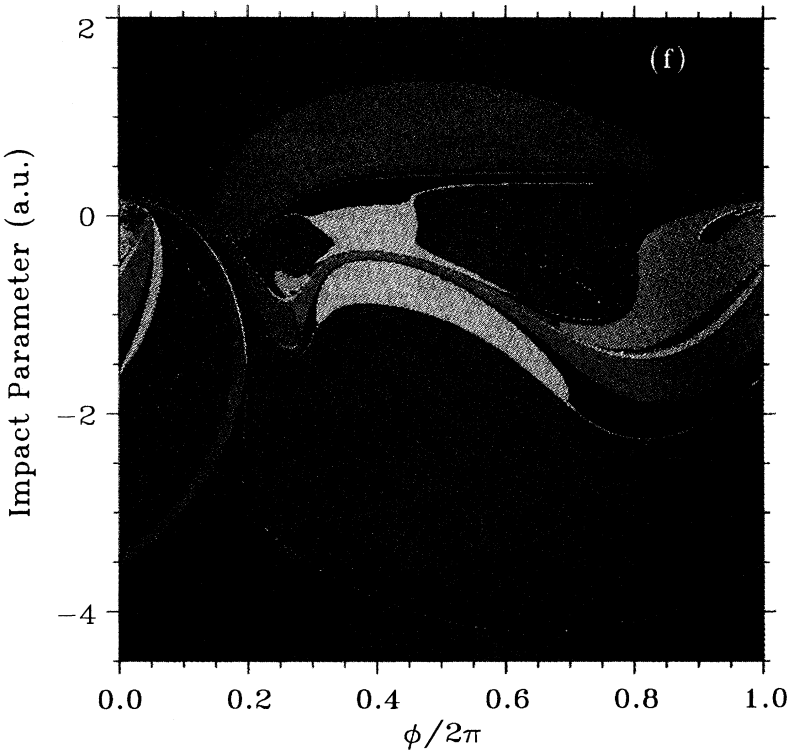

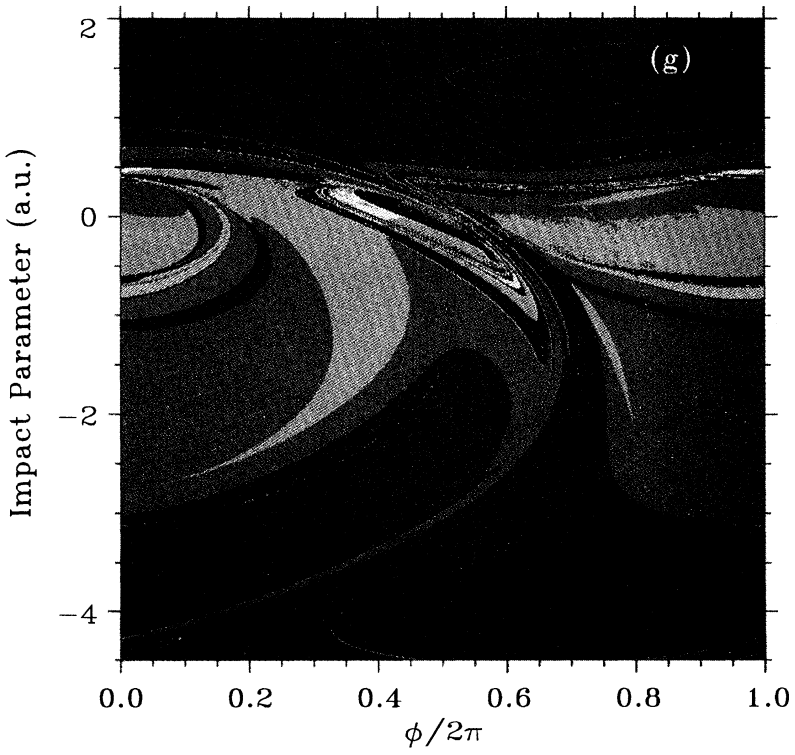

FIG. 1. (*Continued*).

ted in the parameter space maps is

$$\phi=\phi_0+\frac{v_0}{r_0}t_0 \ . \tag{4}$$

This definition corresponds to the phase angle [shown in Fig. 1(b)] that the electron would have at closest approach of the nuclei (i.e., at $t=0$) if there were no interaction between the projectile and the target electron. (Alternatively, it is possible to vary ϕ, holding ϕ_0 fixed by changing t_0. This is equivalent to changing the initial distance of the projectile from the target.)

B. Exit tests

After each trajectory has been integrated, exit tests are performed to determine the outcome of the collision event. The first test determines whether the electron is closer to the target or to the projectile after the collision. If the electron is closer to the target, then the energy ϵ_t (kinetic plus potential) of the electron relative to the target rest frame is compared with the saddle point potential energy $\epsilon_s \equiv -4/R$, with R the internuclear separation in units of r_0. If $\epsilon_t < \epsilon_s$, then we conclude that neither capture nor ionization occur for this trajectory and we label the trajectory as an inelastic scattering event. If the electron is closer to the projectile, its energy ϵ_p relative to the projectile rest frame is compared with ϵ_s. If $\epsilon_p < \epsilon_s$, then the collision event results in capture. If the energy relative to the closest center is positive, then the event results in ionization of the electron.

For a small number of trajectories, the energy relative to the closest center will be negative but greater than ϵ_s. In this case, the equations are integrated to larger internuclear separations to determine whether the electron is subsequently captured by either nucleus. The exit tests are then repeated at times equal to integral multiples of t_f, until a definite outcome can be assigned to the trajectory. This procedure is repeated, up to time $t=6t_f$, and if convergence is not achieved at that point the outcome is labeled unknown and is represented in the parameter space maps by a *black* pixel.

IV. CLASSICAL COLLISION CHANNELS

A. Binary encounter ionization

The simplest parameter space maps are observed at high velocities, where the collision time is short compared with the orbital period of the electron. In this regime, ionization by binary encounter [21] is the dominant reaction mechanism aside from scattering. Figure 1(c) is a parameter space map for coplanar collisions (two dimensional) at a reduced velocity, $\bar{v}=V_p/v_0=10$. Note that the electron orbit is aligned so that $\hat{\mathbf{l}}=\hat{\mathbf{k}}$, i.e., the electron moves in a counterclockwise direction, as indicated in Fig. 1(b). The map consists predominantly of scattering events in which the electron remains bound to the target, but a sinusoidal band of ionization events correlates the impact parameter with the initial phase of the slowly moving electron in its orbit; note that $\sin\phi$ is the projection of the electron's position vector onto the $\hat{\mathbf{j}}$ axis at closest approach of the nuclei. The width of this ionization band increases with decreasing ion velocity, as will be apparent in subsequent maps. As the collision time increases, the impulse experienced by the electron increases, so that more distant binary encounters can lead to ionization.

Remnants of binary-encounter ionization are apparent even at much lower collision velocities, as can be seen in Figs. 1(d) and 1(e). In these maps, corresponding to $\bar{v}=4$ and 2, the sinusoidal band has widened, particularly at negative impact parameters where the electron and ion are comoving at closest approach.

B. Thomas scattering

Figures 1(d) and 1(e) also show the emergence of capture processes in the midst of the ionization zone. Thomas described a high-velocity capture mechanism due to a double scattering of the electron [14]. The electron first scatters from the incoming ion at an angle of 60° with respect to the beam axis and it acquires the speed of the ion. The electron then scatters from the target ion and emerges in the beam direction with nearly zero velocity relative to the projectile. This three-swap Thomas mechanism for electron capture is identified as two small red regions in the parameter space map shown in Fig. 1(d). This map was obtained for coplanar collisions at a reduced ion velocity of $\bar{v}=4$. The plot shows a blue sinusoidal shape, as in Fig. 1(c), corresponding to ionization of the target electron by a binary encounter with the projectile. The sine wave has broadened and two small red capture regions have appeared near $\phi=120°$ and 240°. These small regions contain three-swap capture events, which correspond to the Thomas mechanism at high velocities. Figure 2 shows a typical trajectory that leads to

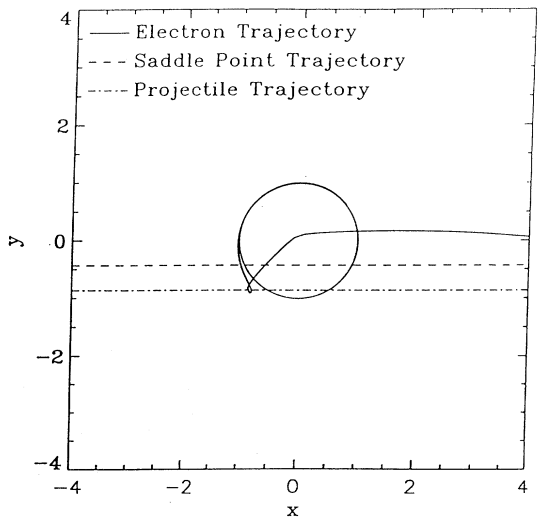

FIG. 2. A typical electron trajectory (solid line) in the Thomas-capture region in Fig. 1(d) for $b=-0.866$ and $\phi/2\pi=0.697$ at $\bar{v}=4$. The dashed and dot-dash lines represent the saddle-point and projectile trajectories, respectively. The scale of length is defined as the initial radius of the orbit.

a Thomas-like capture for a reduced ion velocity of $\bar{v}=4$. The solid, dashed, and dot-dash lines represent the trajectories of the electron, saddle point, and projectile, respectively. This electron trajectory corresponds to the single point $b=-0.866$ and $\phi=240°$, which is roughly in the center of the three-swap zone in Fig. 1(d). [There are Thomas capture processes at $\bar{v}=10$, though they are too few to be seen in Fig. 1(c).] The three-swap captures are found to emerge from the binary encounter zone as the ion velocity decreases. The two zones of three-swap capture grow as the reduced velocity decreases to $\bar{v}=1$.

C. Direct capture

Direct-capture processes correspond to electron trajectories that pass only once through the midplane separating the charge centers. Like three-swap capture, direct capture also emerges out of the ionization zone, as can be seen in the parameter space map for reduced velocity $\bar{v}=2$, shown in Fig. 1(e). Direct capture—or one-swap—trajectories, appear in Fig. 1(e) as a zone of dark red in a region of the map where the electron and projectile are comoving, i.e., where the velocities of both the electron and the projectile have roughly the same magnitude and direction [22,5]. This region appears to grow at the expense of ionization as we continue to lower the reduced velocity. This same tendency is apparent for the three-swap capture zones, which are now considerably larger than in Fig. 1(d). At the matching velocity $\bar{v}=1$, the parameter space map shown in Fig. 1(f) is now quite complex, though the one-swap capture events now dominate both three-swap capture and ionization, which are restricted mostly to small impact parameters. The relative contributions of one-swap and three-swap trajectories to the charge-transfer cross sections were discussed in detail in our earlier study [9].

D. Saddle-point ionization

Recall that the ionization region of the parameter space maps has been subdivided into zones determined by comparing the final velocity vector of the electron with the velocity vectors of the target ion, projectile ion, and saddle point. Saddle-point ionizations are *defined* here as those events for which the final speed (at $t=t_f$) of the electron relative to the saddle is smaller than its speed with respect to either of the charge centers. These events are represented by the darkest shade of blue in Figs. 1(c)–1(g). One might think that our definition of saddle-point ionization events is sensitive to our arbitrary choice of t_f; however, numerical tests in which t_f is increased by two orders of magnitude show no substantial changes in the parameter space maps.

Figure 3 shows a typical trajectory that leads to saddle-point ionization for a reduced ion velocity of $\bar{v}=2$. This trajectory corresponds to the single point $b=-2.0$ and $\phi=\pi$, which is roughly in the center of the ionization zone of Fig. 1(e). As the saddle point approaches the electron's circular orbit, the net force on the electron becomes small and the electron leaves its orbit in a direction nearly perpendicular to the beam axis; its speed at this point is still comparable to its initial value. As the electron moves off the saddle it experiences a rapidly decreasing net force in the direction of the saddle as the ions separate. The net force deflects the electron slightly in the forward direction, and it eventually emerges at a small angle with respect to the beam axis. Actual determination of the angle would require integration to extremely large times [23]. These characteristics of saddle-point ionization events were noted earlier by Irby [24].

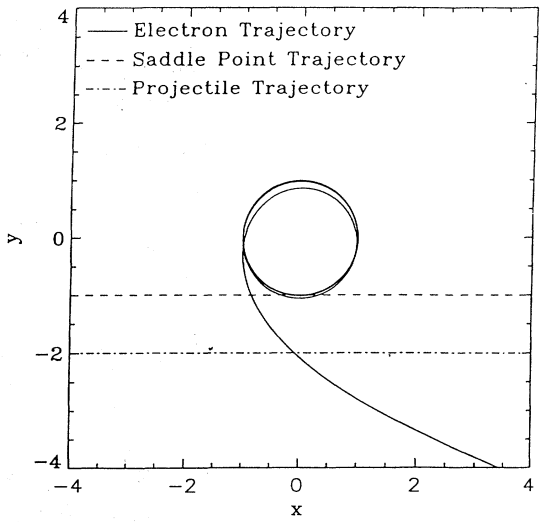

FIG. 3. A typical electron trajectory (solid line) in the saddle-point region in Fig. 1(e) for $b=-2.0$ and $\phi/(2\pi)=\frac{1}{2}$ at $\bar{v}=2$. The dashed and dot-dashed lines represent the saddle-point and projectile trajectories, respectively. The scale of length is defined as the initial radius of the orbit.

Saddle-point ionization events dominate all other ionization processes when the speed of the saddle point $\frac{1}{2}V_p$ is comparable to the speed of the target electron, i.e., at a reduced velocity of $\bar{v}=2$, as is apparent in Fig. 1(e). At higher velocities, where binary-encounter ionizations dominate [Figs. 1(c) and 1(d)], the speed of the ejected electron is smallest with respect to the target. At the matching velocity $\bar{v}=1$ [Fig. 1(f)], the ionization events are roughly equally distributed among the three centers.

To test our model's assumption of infinite nuclear masses, we have solved the equations of motion for a full three-body collision between a pointlike sodium ion and a circular Keplerian lithium atom at $\bar{v}=1.0$. Comparing the full three-body result shown in Fig. 4(a) to Fig. 1(f), we find only minute changes in the parameter space maps. These small differences stem from changes in the final velocity vectors of the ions, relative to which the velocity of the ionized electron is being compared. Nevertheless, the number of ionization events of each type is essentially the same as with infinite nuclei. Figure 4(b) shows a similar map generated for a proton incident on a circular-state hydrogen atom. This figure shows a discontinuity about zero impact parameter that results from Rutherford scattering, but is otherwise identical to the infinite mass case.

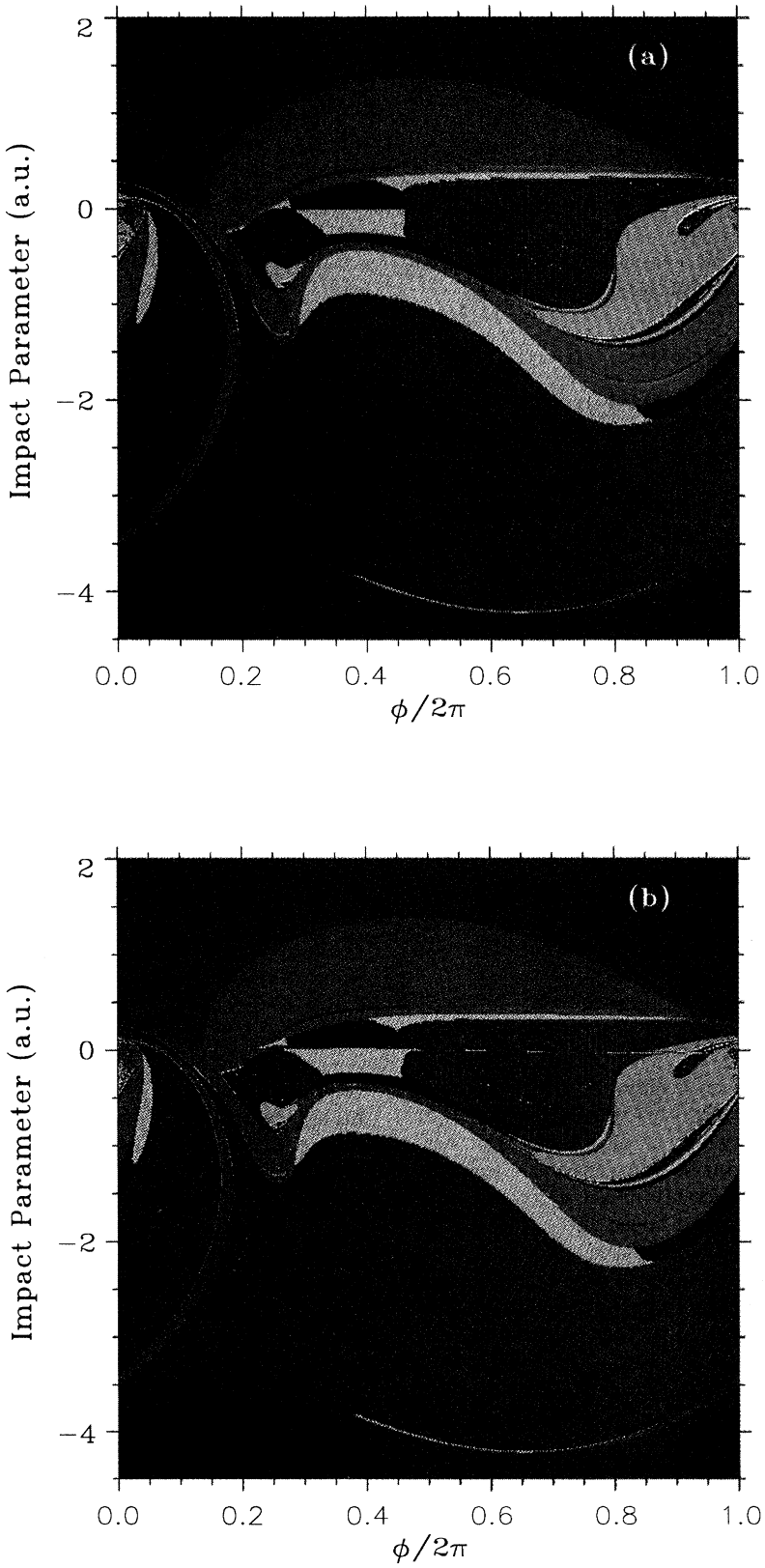

FIG. 4. The same as Fig. 1(f) for a three-body calculation of a structureless, singly charged ion of mass 23 amu ("Na^+") incident on a circular-state Li* Rydberg atom whose singly charged core has mass 7 amu ("Li") (a). The same as Fig. 1(f) for a three-body calculation of a proton incident on a circular-state H* Rydberg atom (b).

E. A superpromotion ionization

While capture events are rare in the limit of high velocities, ionization events are rare in the limit of low projectile velocities. As was the case with Thomas capture, such rare events might be expected to occur only for a specific set of initial conditions. Interpretation of the parameter space zones corresponding to ionization at low velocities is complicated by the severe distortion of the initial orbit as the ion approaches the target. The usefulness of the phase parameter ϕ and the means by which it was standardized [Eq. (3)] are less obvious in the adiabatic limit, where the duration of the collision is large compared to the period of the initial orbit. Interpreting the parameter space maps at low velocities often requires extensive plotting of characteristic orbits from each of the observed zones.

Figure 1(g) displays a complicated map of final collision channels for $\tilde{v}=0.5$, dominated by charge transfer and excitation for infinite-mass nuclei. Even though the map has lost the identifiable features found at higher ion velocities, the ionization regions have become smaller and localized near small impact parameters. The darkest shade of blue, which labels those ejected electrons traveling at or near the saddle speed, are barely discernible in this figure. We find that ionization in this region occurs primarily on the incoming stage of the collision, which is reminiscent of S superpromotion ionization found in adiabatic collisions between ions and targets in low angular momentum states [25]. The S superpromotion ionization channels are related to an unstable trajectory of the electron located on top of the centrifugal barrier [26].

V. CONCLUSIONS

We have revisited the Newtonian mechanics of ion-atom collisions in search of the classical analogs of a number of well-known mechanisms for excitation, ionization, and charge transfer. Our study is motivated by the experiments of Refs. [5] and [7] on charge transfer from circular and elliptical state targets. The preparation of target states with both high principal quantum number and high angular momentum quantum numbers suggests that a classical interpretation of the dominant features of collision cross sections may be possible. The results of our earlier work [9] indicate that this is, in fact, the case, at least for total charge-transfer cross sections and at ion speeds above the velocity of the target electron.

To supplement the results of our earlier study we have presented here a detailed look at that part of the phase space that seems most relevant to collisions from circular states. While we have only presented parameter space maps corresponding to coplanar collisions, we have generated many such maps for different orientations of the orbit (and also for elliptical orbits.) The primary value of these maps, in our view, is that they indicate that there are only two pathways to charge transfer for projectile speeds above the speed of the target electron, and that these pathways are localized in separate regions of the initial condition parameter space. The two pathways are topologically distinguished simply by counting the number of swaps for each trajectory. We have shown that the three-swap pathway coincides with the Thomas mechanisms at high velocities, and that the one-swap pathway results from a propensity for capture of comoving electrons.

In addition, our parameter space maps illustrate the mass independence of collision dynamics at intermediate velocities. Even a cursory comparison of Figs. 4(a), 4(b), and 1(f) suggests that the infinite nuclei approximation is adequate for interpreting the results of experiments with alkali-metal-projectile ions and alkali-metal target atoms.

ACKNOWLEDGMENTS

We thank Alan D. MacKellar and Jamie C. Day for sharing technical expertise concerning trajectory calculations for few-body systems. We also are grateful for helpful discussions with and suggestions from Keith B. MacAdam and Victor D. Irby. Research supported by the Division of Chemical Sciences, Office of Basic Energy Sciences, Office of Energy Research, U. S. Department of Energy.

[1] See K. B. MacAdam, in *Abstracts of Contributed Papers, Eighteenth International Conference on the Physics of Electronic and Atomic Collisions,* edited by T. Andersen, B. Fastrup, F. Folkmann, and H. Knudsen (IFA, Aarhus University, Aarhus, 1993), Vol. 2, p. 725.

[2] D. Delande and J. C. Gay, Europhys. Lett. **5**, 303 (1988).

[3] J. Hare, M. Gross, and P. Goy, Phys. Rev. Lett. **61**, 1938 (1988).

[4] J. C. Day *et al.*, Phys. Rev. Lett. **72**, 1612 (1994).

[5] S. B. Hansen *et al.*, Phys. Rev. Lett. **71**, 1522 (1993).

[6] T. Ehrenreich, *et al.*, in *Abstracts of Contributed Papers, Eighteenth International Conference on the Physics of Electronic and Atomic Collisions,* edited by T. Andersen, B. Fastrup, F. Folkmann, and H. Knudsen (IFA, Aarhus University, Aarhus, 1993), Vol. 2, p. 725.

[7] T. Ehrenreich, J. C. Day, S. B. Hansen, E. Horsdal-Pedersen, K. B. MacAdam, and K. S. Morgensen, J. Phys. B **27**, L383 (1994).

[8] J. Wang and R. E. Olson, Phys. Rev. Lett. **72**, 332 (1994).

[9] D. M. Homan, M. J. Cavagnero, and D. A. Harmin, Phys. Rev. A **50**, R1965 (1994).

[10] R. Abrines and I. C. Percival, Proc. Phys. Soc. **88**, 861 (1966).

[11] R. E. Olson and A. Salop, Phys. Rev. A **16**, 531 (1977).

[12] C. O. Reinhold and C. A. Falcon, J. Phys. B **21**, 2473 (1988).

[13] R. E. Olson, Phys. Rev. A **27**, 1871 (1983).

[14] L. H. Thomas, Proc. R. Soc. London **114**, 561 (1927).

[15] G. H. Wannier, Phys. Rev. **90**, 817 (1953).
[16] J. C. Day, Bull. Am. Phys. Soc. **37**, 1097 (1992).
[17] V. Daniel, M. Vallieres, and J. Yuan, Chaos **3**, 475 (1993).
[18] P. Hut, Astron. J. **88**, 1549 (1983).
[19] P. T. Boyd and S. L. W. McMillian, Chaos **3**, 507 (1993).
[20] W. H. Press, B. P. Lannery, S. A. Teukolsky, and W. T. Vetterling, *Numerical Recipes* (Cambridge University Press, New York, 1989).
[21] J. J. Thomson, Philos. Mag. **23**, 449 (1912).
[22] G. A. Kohring, A. E. Wetmore, and R. E. Olson, Phys. Rev. A **28**, 2526 (1983).
[23] David Schultz (private communication).
[24] V. D. Irby, Phys. Rev. A **39**, 54 (1989).
[25] E. A. Solov'ev, Zh. Eksp. Teor. Fiz. **81**, 1681 (1981) [Sov. Phys. JETP **54**, 893 (1981)].
[26] D. I. Abramov, S. Yu. Ovchinnikov, and E. A. Solov'ev, Phys. Rev. A **42**, 6366 (1990).

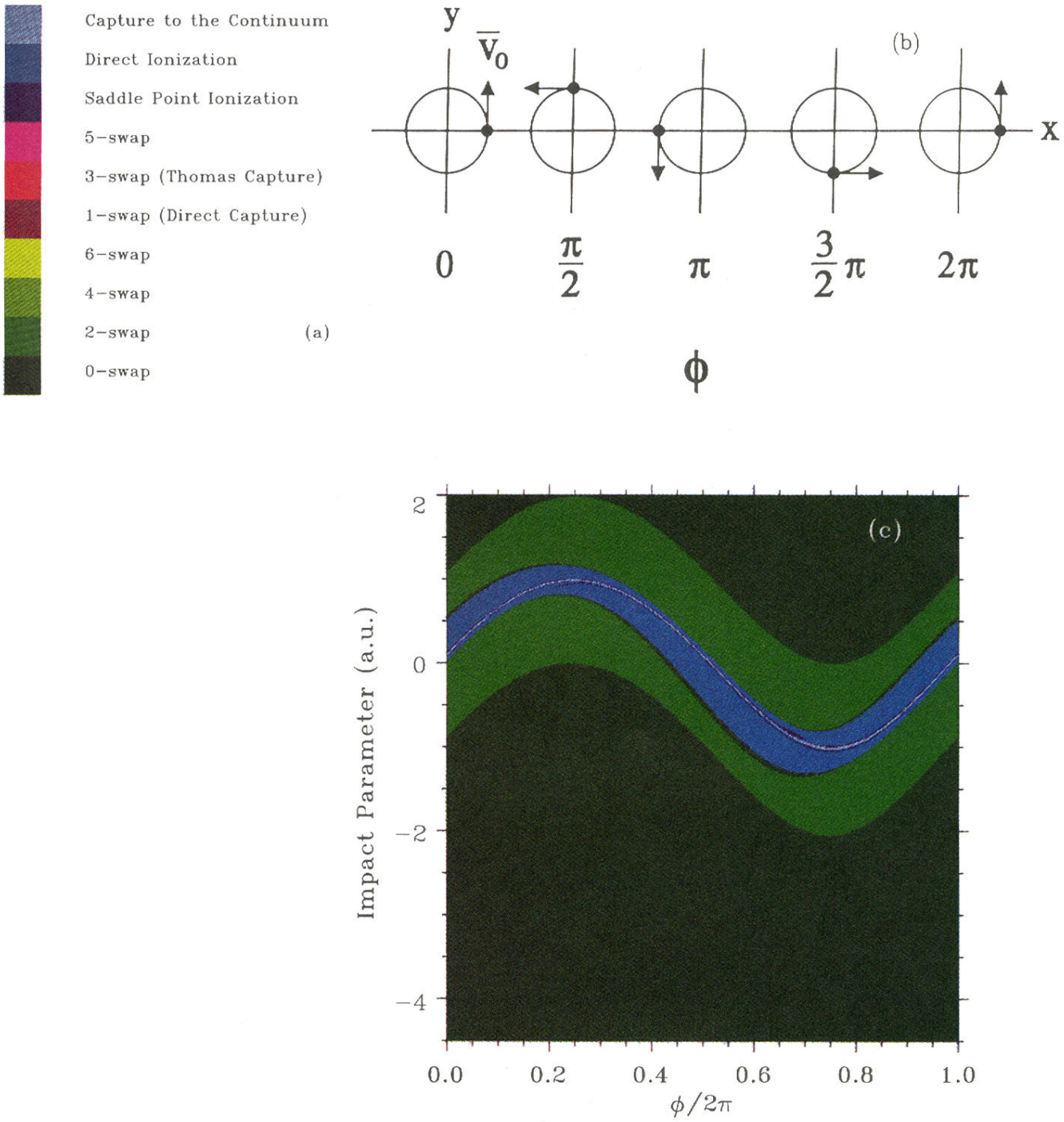

FIG. 1. Parameter space maps for coplanar collisions. These plots correlate the impact parameter and the initial phase angle ϕ of the electron's circular orbit with specific outcomes as specified in the color chart (a). The phase angle ϕ of the electron is standardized [Eq. (4)] so that, in the absence of projectile target interaction, the electron position at $t=0$ would be as shown in (b). Collision outcomes represented by a color pixel for each of 250 000 trajectories are shown for reduced ion velocities of (c) $\bar{v}=10.0$, (d) $\bar{v}=4.0$, (e) $\bar{v}=2.0$, (f) $\bar{v}=1.0$, and (g) $\bar{v}=0.5$.

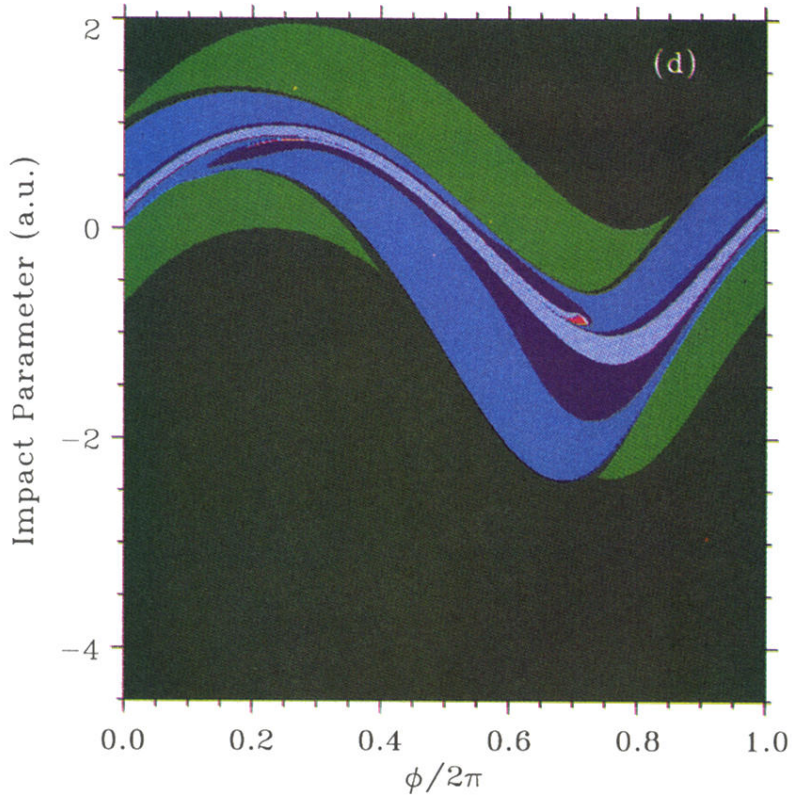

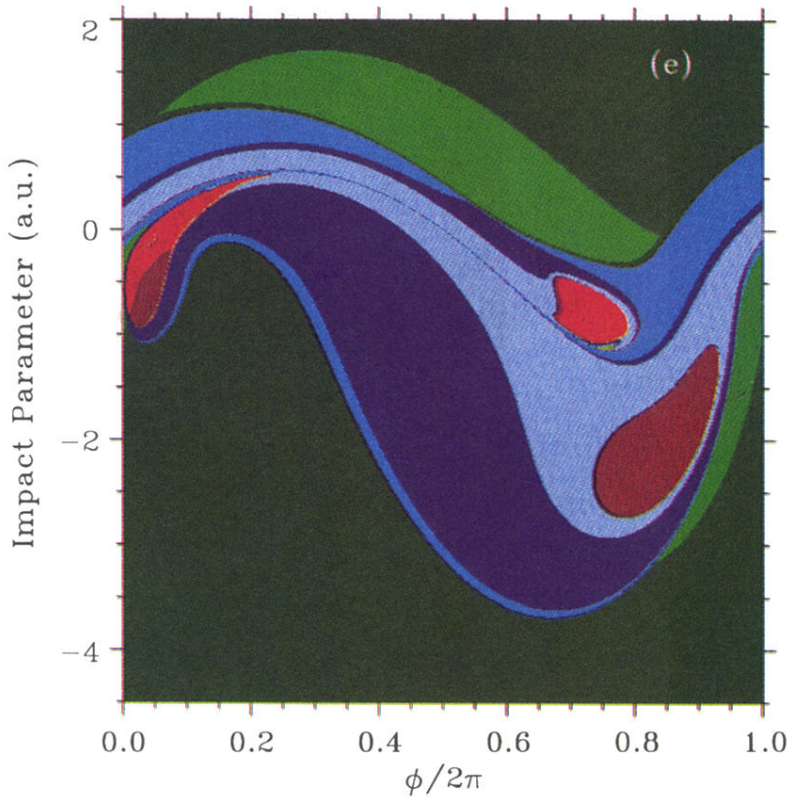

FIG. 1. (*Continued*).

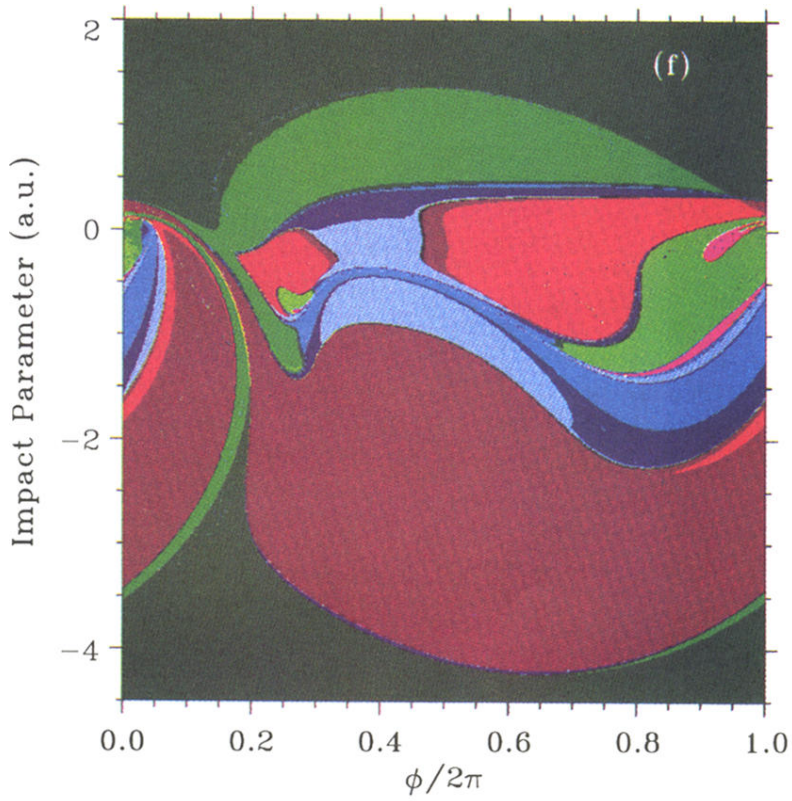

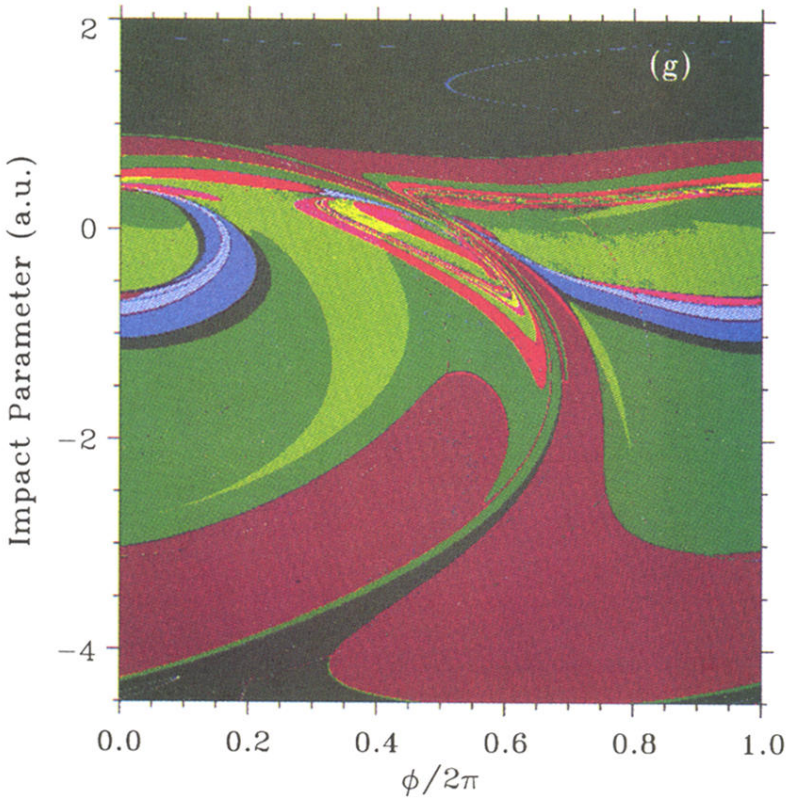

FIG. 1. (*Continued*).

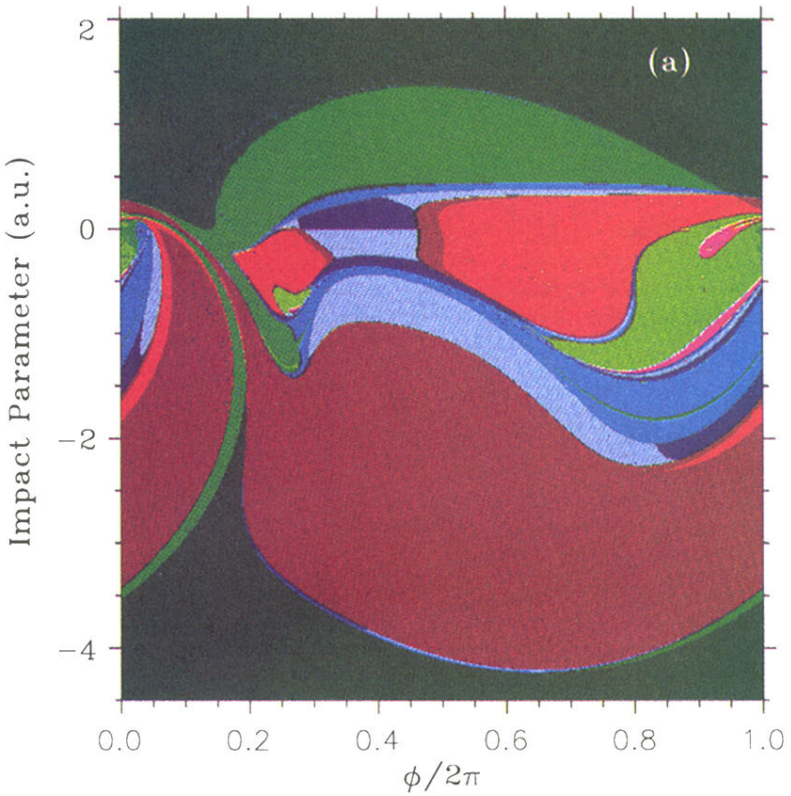

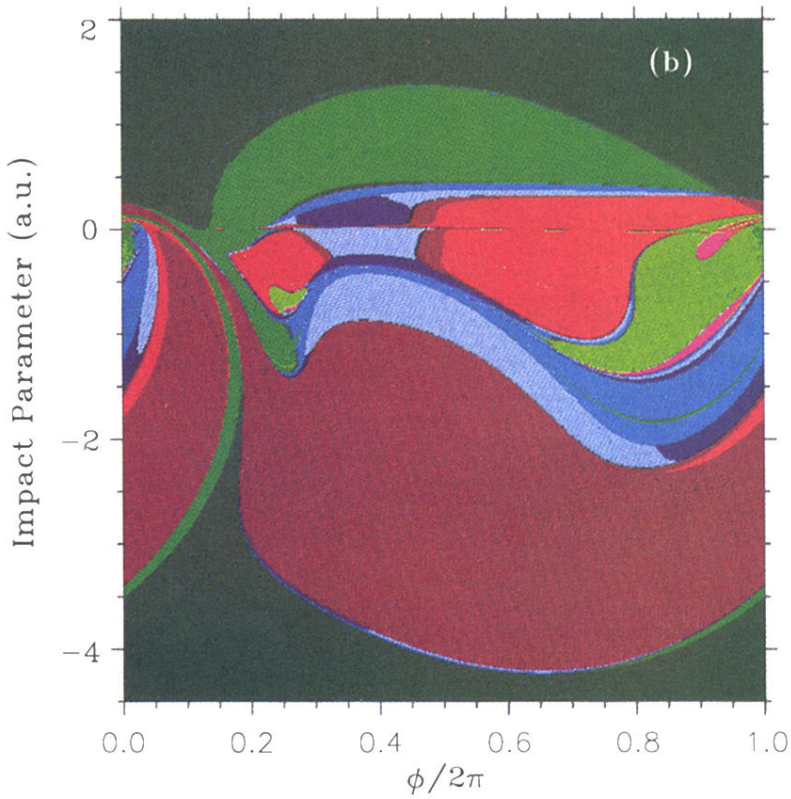

FIG. 4. The same as Fig. 1(f) for a three-body calculation of a structureless, singly charged ion of mass 23 amu ("Na^+") incident on a circular-state Li^* Rydberg atom whose singly charged core has mass 7 amu ("Li") (a). The same as Fig. 1(f) for a three-body calculation of a proton incident on a circular-state H^* Rydberg atom (b).